Supporting Information

Elucidating the Reactivity and Mechanism of CO_2 Electroreduction at Highly Dispersed Cobalt Phthalocyanine

Minghui Zhu[§], Ruquan Ye[§], Kyoungsuk Jin, Nikifar Lazouski, and Karthish Manthiram[*]

[1]Department of Chemical Engineering, Massachusetts Institute of Technology, Cambridge, MA 02139, USA

[*]Correspondence: karthish@mit.edu

[§] These authors contributed equally to this work

Table of Contents

Experimental methods

Preparation of electrodes. Disc shaped electrodes with a diameter of 0.5 inches were punched from carbon paper (Toray, TGP-H-060, Fuel Cell Earth LLC) and heated in a tube furnace at 780°C in static air for 20 min to generate oxygen-functionalized carbon paper (OxC). Catalyst ink was prepared by dispersing 10 mg of CoPc (Sigma Aldrich, β-form, dye content 97%) in a mixture of 100 μL of 5 wt.% Nafion solution (Sigma Aldrich, Nafion 117, 5 wt. %) and 1900 μL N,N-dimethylformamide (DMF, Sigma Aldrich, 99.8%) with 1 hour of sonication. This solution was then serially diluted in DMF to obtain catalyst inks containing CoPc concentrations ranging from 2.5×10^{-4} to 5 mg/ml, with the corresponding Nafion content ranging from 1.07×10^{-4} to 2.14 mg/ml. The CoPc/OxC working electrode was then prepared by dropcasting 15 μL of the prepared ink onto the center of OxC. The droplet instantaneously spread throughout the entire carbon paper without penetrating onto the underlying aluminum foil. The electrode was left undisturbed under ambient conditions for 30 min and then oven-dried in air at 80°C for 1 h.

For control experiments designed to test the effect of deposition solvent on catalyst dispersion and TOF, we used isopropanol (VWR, 99% Semi Grade) in place of N,N-dimethylformamide (Sigma Aldrich, 99.8%). To determine the impact of oxygen-containing functional groups, we omitted the heating treatment and used this pristine carbon paper (CP) as support.

Materials characterization. SEM/EDX was performed on a Zeiss Merlin High-resolution scanning electron microscope with an InLens detector.

Electrochemical characterization. Electrochemical measurements were conducted in a customized three-compartment cell (Fig. S7) fabricated from polycarbonate, containing a counter electrode compartment, working electrode compartment, and gas compartment. The working electrode compartment was separated from the counter electrode compartment by a Selemion membrane (AGC Engineering, AMV). The counter and reference electrodes were platinum foil (99.9% metals basis, Alfa Aesar) and Ag/AgCl (LF-2, Innovative Instrument Inc.), respectively. CoPc/OxC electrode was placed between the working electrode compartment and gas compartment.

Prior to experiments, 1.75 mL of electrolyte of specified composition was added into the working electrode compartment and counter electrode compartment, respectively. A magnetic stir bar was placed into the working electrode compartment and stirred at a speed of 200 rpm to facilitate reactant/product convection. High-purity CO_2 gas (Airgas, 99.999%, 10 sccm) was controlled by Alicat mass flow controller and introduced into the cell at atmospheric pressure; CO_2 gas enters the cell through the gas compartment, traverses the working electrode, and exits through the working electrode compartment. Cells were purged with CO_2 for 10 min before electrochemical polarization.

The electrochemical measurements were controlled with a VMP3 Multi-channel potentiostat. Resistance between the reference and working electrodes was measured with Potential Electrochemical Impedance Spectroscopy (PEIS) and manually compensated by 85%. For the experiments where CO_2 partial pressure was varied, the total flow rate and pressure were kept constant by adding in a diluent stream of nitrogen. Tafel slope and order-dependence measurements were conducted by holding at desired potential steps for 15 minutes each, with gas products analyzed by an on-line gas chromatograph (SRI Instruments) every 5 minutes. The gas chromatograph was equipped with TCD and FID detectors, a methanizer, and a Hayesep-D column.

Sodium bicarbonate electrolytes, of molarity ranging from 0.1 M to 1 M, were prepared by bubbling CO_2 (Airgas, 99.999% research grade) through sodium carbonate (Sigma Aldrich, 99.999% trace metal basis) solution overnight. To test the order dependence on bicarbonate at constant ionic strength, sodium perchlorate (Sigma Aldrich, ≥ 98.0%) was used as supporting electrolyte. Sodium perchlorate poses an explosion hazard and should only be used with appropriate training and safety precautions. In these experiments, for a desired sodium bicarbonate concentration, the total sodium ion concentration was kept at 1 M by varying the sodium perchlorate concentration.[1]

Electrolysis of CoPc/OxC under CO_2 and N_2

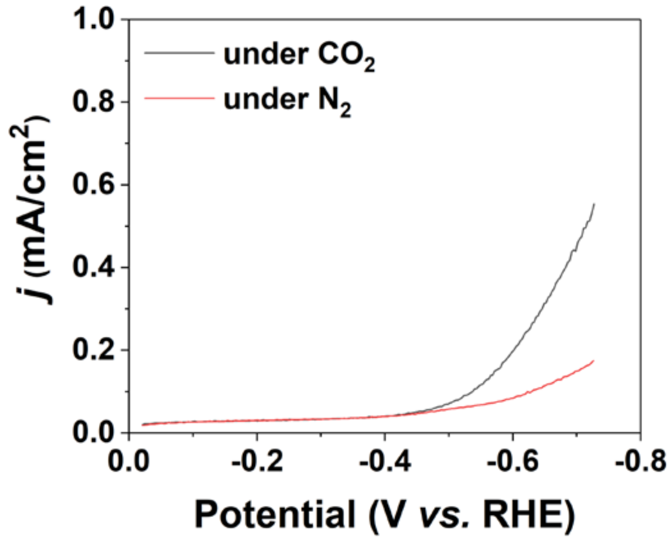

Figure S1. Linear sweep voltammetry collected at a sweep rate of 50 mV/s at CoPc/OxC with a loading of 1×10^{-11} mol/cm^2 under CO_2 and N_2, respectively, in 0.1M $NaHCO_3$.

Long term stability test

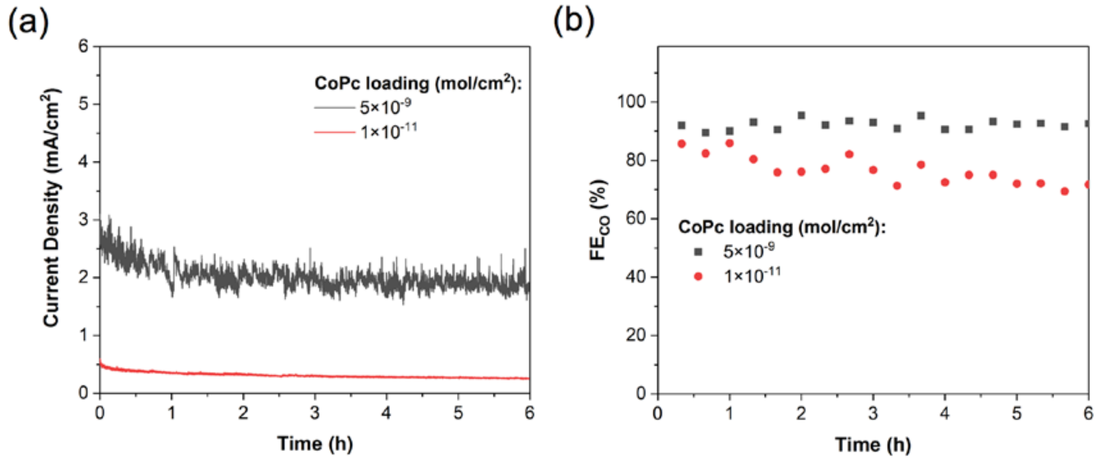

Figure S2. Long term stability test of CoPc/OxC (loading: 5×10^{-9} mol/cm^2 and 1×10^{-11} mol/cm^2) in 0.1 M $NaHCO_3$ at -0.73 V *vs.* RHE. (a) Current densities and (b) Faradaic efficiencies for CO. The current densities at higher loadings generally exhibit larger fluctuations, likely due to bubble formation.

Additional SEM image

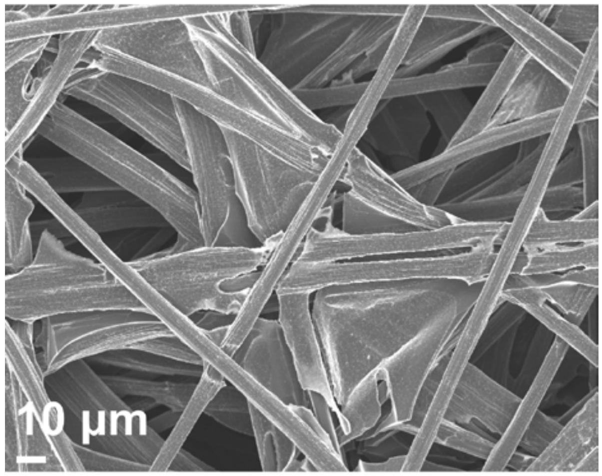

Figure S3. SEM image of CoPc/OxC (loading: 1 x 10^{-9} mol/cm^2) showing no crystals.

Electrode preparation control experiments

To elucidate the essential factors involved in achieving high TOFs, the effect of the solvent for catalyst ink as well as the oxygen-containing functional groups on the carbon paper were evaluated through a series of control experiments (Fig. S4). The blank oxygen-functionalized carbon paper (OxC) with no loaded CoPc catalyst produced negligible CO under the tested potentials (Table S2), helping to exclude direct reduction of carbon dioxide by the support. For CoPc/OxC electrodes cast from isopropanol, the TOFs are less than those when DMF was used as solvent. This is likely due to the improved CoPc solubility in DMF that provides better dispersion of the catalyst. The importance of oxygen-containing functional groups is evident upon switching from OxC to untreated carbon paper (CP), which does not involve a high temperature treatment in air to drive incorporation of oxygen-containing functional groups. Here, isopropanol is used as common solvent as DMF solution does not wet untreated carbon paper due to its hydrophobicity (Fig. S5). Use of CP as opposed to OxC leads to TOFs that decreased by an order of magnitude and do not increase at lower loadings of CoPc. This indicates the importance of the oxygen-containing functional groups in facilitating dispersion of the catalyst, possibly by weak coordination between oxygen atoms and Co^{II} centers that reduces the self-stacking of CoPc molecules. These control experiments indicate the importance of controlling both the polarity of the solvent and oxophilicity of the support for achieving high catalyst dispersion.

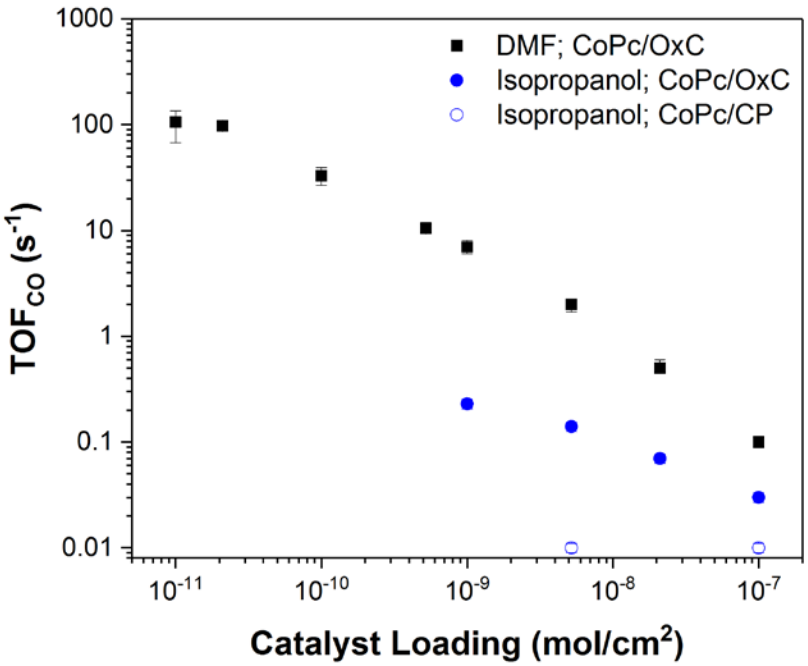

Figure S4. TOF as a function of CoPc loadings in 0.1 M $NaHCO_3$ at -0.73 V *vs.* RHE. Black solid squares represent CoPc/OxC prepared with DMF as solvent from which catalyst is dropcasted. Blue solid circles represent CoPc/OxC with isopropanol as solvent from which catalyst is dropcasted. Blue hollow circles represent CoPc/CP with isopropanol as dropcasting solvent and use of CP as support instead of OxC.

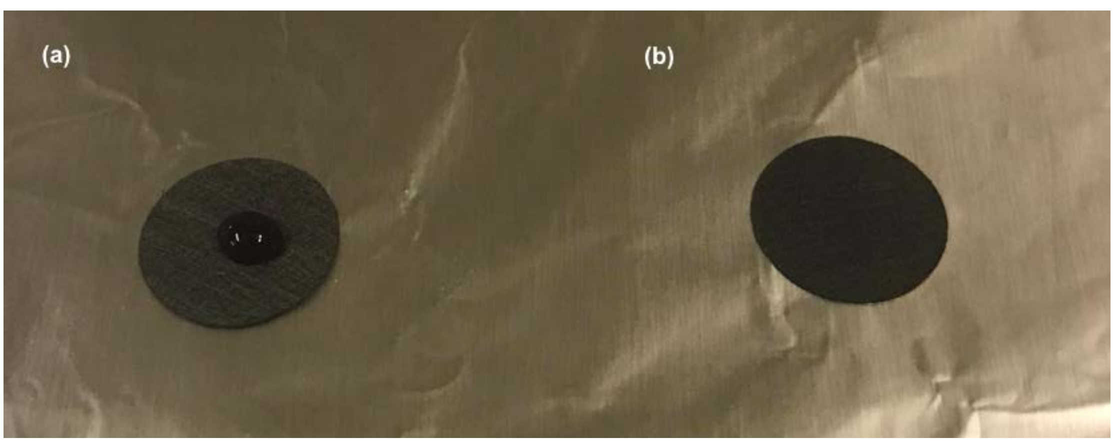

Figure S5. (a) Pristine carbon paper (CP) and (b) oxygen functionalized carbon paper (OxC) with 15μL of CoPc/Nafion/DMF solution dropcasted.

Tafel slopes

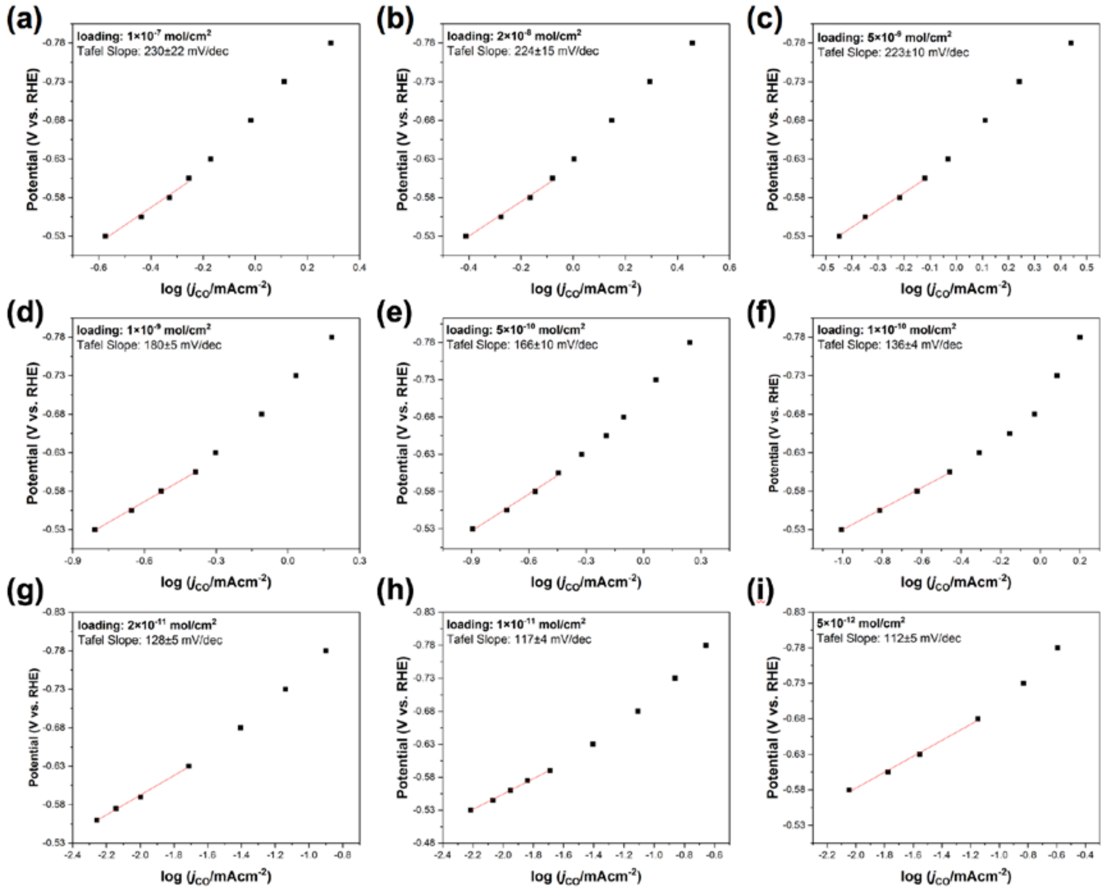

Figure S6. Tafel plot for CoPc/OxC (a. 1×10^{-7} mol/cm^2, b. 2×10^{-8} mol/cm^2, c. 5×10^{-9} mol/cm^2, d. 1×10^{-9} mol/cm^2, e. 5×10^{-10} mol/cm^2, f. 1×10^{-10} mol/cm^2, g. 2×10^{-11} mol/cm^2, h. 1×10^{-11} mol/cm^2, i. 5×10^{-12} mol/cm^2) in 0.1 M $NaHCO_3$ electrolyte.

Electrochemical cell design

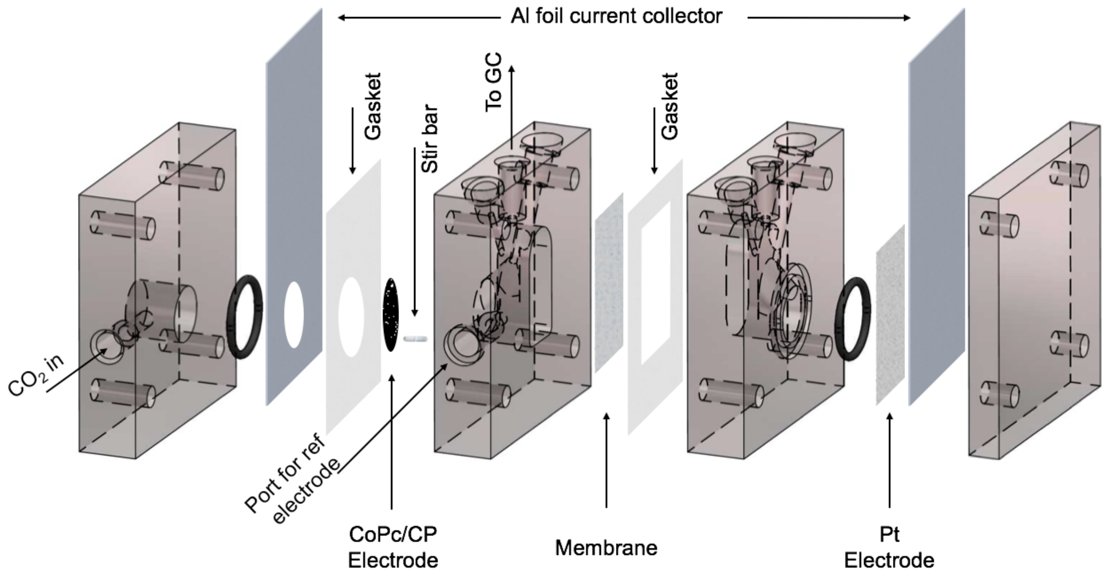

Figure S7. Schematic of the 3-compartment electrochemical cell and setup used in the present study.[2]

Bicarbonate order dependence at more reducing potential

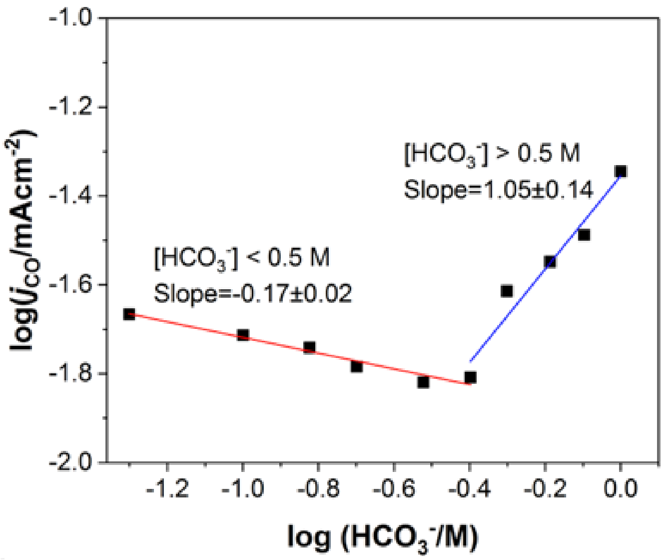

Figure S8. CO partial current density (j_{CO}) as a function of bicarbonate concentration for CoPc/OxC (1 x 10^{-11} mol/cm^2) at -0.63 V *vs.* RHE.

Current density and Faradaic efficiency data

Table S1. Detailed current densities and Faradaic efficiencies for CoPc/OxC catalysts at -0.73 V *vs.* RHE in 0.1 M $NaHCO_3$ electrolyte.

Loading (mol/cm^2)	***j*** **(mA/cm^2)**	**FE_{CO} (%)**	**FE_{H2} (%)**
1×10^{-7}	2.4	96 ± 3	4 ± 1
2×10^{-8}	2.7	94 ± 1	6 ± 1
5×10^{-9}	2.6	93 ± 1	8 ± 3
1×10^{-9}	1.9	86 ± 1	12 ± 2
5×10^{-10}	1.5	86 ± 1	14 ± 2
1×10^{-10}	0.9	85 ± 3	12 ± 1
2×10^{-11}	0.6	85 ± 1	15 ± 1
1×10^{-11}	0.3	80 ± 4	16 ± 4

Electrolysis on blank carbon paper

Table S2. Control experiments with high temperature treated carbon paper (OxC) as a working electrode, with no deposited catalyst. The small background current densities for CO confirm that deposited CoPc is the primary catalyst in this study and indicates that background correction of measured currents is not necessary.

Potential (V *vs.* RHE)	**j_{CO} (mA/cm^2)**	**j_{H2} (mA/cm^2)**
-0.57	0	0
-0.63	0	0.003
-0.68	0	0.006
-0.73	0.006	0.014

Comparison of reported turnover frequencies

Table S3. A comparison of reported molecular catalysts for the electroreduction of CO_2 to CO in aqueous media to CoPc/OxC investigated in this study. NR indicates that the value is not reported.

Catalyst	*j* (mA/cm^2)	V *vs.* RHE	Electrolyte (pH)	FE_{CO}(%)	TOF_{CO}(s^{-1})	Ref.
CoPc/OxC (2×10^{-8} mol/cm^2)	2.7	-0.73	0.1M $NaHCO_3$ (6.8)	94	0.5	This Study
CoPc/OxC (1×10^{-11} mol/cm^2)	0.34	-0.73	0.1M $NaHCO_3$ (6.8)	80	113	This Study
CoPc/OxC (1×10^{-11} mol/cm^2)	1.0	-0.73	1M $NaHCO_3$ (7.8)	90	400	This Study
CoTPP/CNT	NR	-0.70	0.5M $KHCO_3$ (7.2)	~70	2.75	[3]
CoPc/CNT	~10.0	-0.63	0.1M $KHCO_3$ (6.8)	92	2.7	[4]
CoPc-CN/CNT	~15.0	-0.63	0.1M $KHCO_3$ (6.8)	98	4.1	[4]
CoPc-CN/CNT	~5.6	-0.46	0.5M $KHCO_3$ (7.2)	88	1.4	[4]
CoPc-P4VP	2.0	-0.73	0.1 M NaH_2PO_4 (4.7)	89	4.8	[5]
CoPc(py)-P2VP	1.9	-0.73	0.1 M NaH_2PO_4 (4.7)	83	4.2	[5]
CoPc-F	~6	-0.90	0.5M $KHCO_3$ (7.2)	88	2.05	[6]
CATpyr/CNT	0.24	-0.59	0.5M $KHCO_3$ (7.3)	93	0.04	[7]
Co(ch)/CNT	NR	-0.83	5.0mM Na_2SO4 (4.6)	89	0.04	[8]
$Al_2(OH)_2$TCPP-Co	~1	-0.67	0.5M $KHCO_3$ (7.3)	76	0.06	[9]
COF-367-Co	3.3	-0.67	0.5M $KHCO_3$ (7.3)	91	0.53	[10]
COF-367-Co(1%)	0.45	-0.67	0.5M $KHCO_3$ (7.3)	53	2.6	[10]

Electrolysis in 1.0 M $NaHCO_3$ under N_2 flow

Table S4. Partial current densities for H_2 and CO during steady-state electrolysis on CoPc/OxC (loading: 1×10^{-11} mol/cm^2) under different potentials with only N_2 fed to the electrochemical cell in 1.0 M $NaHCO_3$ electrolyte. The production of CO in the absence of bubbled CO_2 illustrates the pronounced contribution of high concentration of HCO_3^- to $CO_{2(aq)}$.

Potential (V *vs.* RHE)	j_{CO} (mA/cm^2)	j_{H2} (mA/cm^2)
-0.63	0.020	0.035
-0.68	0.032	0.117
-0.73	0.062	0.210
-0.78	0.113	0.468

Kinetic parameters (Tafel slope and order dependence)

Table S5. Proposed mechanism and kinetic parameters for the electrochemical reduction of CO_2 to CO, including the rate-determining step (RDS) in both high and low bicarbonate conditions. The numbers without brackets are theoretical values and the numbers in parentheses are experimentally calculated in this study. The RDS at low bicarbonate concentration involves an electron transfer, while that at high bicarbonate concentration involves a concerted proton-electron transfer. It is possible that the carbon dioxide molecule pre-associates with the active site prior to the electron transfer involved in the rate-determining step.

Condition	**Mechanism**	**Tafel Slope (mV/dec)**	**Reaction order**	
			CO_2	**HCO_3^-**
$[HCO_3^-] < 0.3$ M	1. $Co^{II}Pc + e^- \rightarrow Co^{I}Pc$ 2. $Co^{I}Pc + CO_2 \rightarrow Co^{II}Pc\text{-}COO^-$ **(RDS)** 3. $Co^{II}Pc\text{-}COO^- + H_2O \rightarrow Co^{II}Pc\text{-}COOH + OH^-$ 4. $Co^{II}Pc\text{-}COOH + e^- \rightarrow Co^{II}Pc\text{-}CO + OH^-$ 5. $Co^{II}Pc\text{-}CO \rightarrow Co^{II}Pc + CO$	118 (117)	1 (1.00)	0 (0.17)
$[HCO_3^-] > 0.3$ M	1. $Co^{II}Pc + e^- \rightarrow Co^{I}Pc$ 2. $Co^{I}Pc + CO_2 + HCO_3^- \rightarrow Co^{II}Pc\text{-}COOH + CO_3^{2-}$ **(RDS)** 3.$Co^{II}Pc\text{-}COOH + e^- \rightarrow Co^{II}Pc\text{-}CO + OH^-$ 4.$Co^{II}Pc\text{-}CO \rightarrow Co^{II}Pc + CO$	118 (120)	1 (0.60)	1 (1.40)

Derivation of kinetic parameters (Tafel slope and reaction order)

1. Low HCO_3^- concentration

If reduction of the reactant CO_2 is limited by an irreversible electron transfer step, the reaction rate expressed as a partial current for CO is:

$$j_{CO} = nFk\theta P_{CO_2} \exp\left(\frac{\beta F\eta}{RT}\right)$$

where n is the total number of electron transfers needed to convert CO_2 to CO, F is Faraday's constant, k is the rate constant for the rate-determining step, θ is the surface coverage of vacant Co^{I} active sites, β is the transfer coefficient (assumed to be 0.5), η is the overpotential, R is the gas constant, and T is the temperature. We assume the population of vacant cobalt active sites is approximately equal to the total population of cobalt active sites since the rate determining step involves CO_2 adsorption to a vacant site; this means θ can be considered to be potential independent. In addition, the initial reduction of cobalt ($Co^{II} + e^- \rightarrow Co^{I}$) is considered to be a fast and irreversible step, such that the population of the vacant Co^{I} sites θ can be treated as a constant.

The Tafel slope is given by the partial derivative of the overpotential with respect to the logarithm of current, yielding:

$$\left(\frac{\partial\eta}{\partial \log j_{CO}}\right)_{P_{CO_2}} = \frac{2.3RT}{\beta F} = 118\ \text{mV/dec}$$

Either $[H^+]$ and $[HCO_3^-]$ could be the proton source and cannot be identified with the collected kinetic data. Such a mechanism has a theoretical Tafel slope of 118 mV/dec, a first order dependence on CO_2, and a zeroth order dependence on bicarbonate[1], consistent with the measured 120 mV/dec Tafel slope, 1.00 order dependence on CO_2, and 0.17 order dependence on bicarbonate (Table S5).

2. High HCO_3^- concentration

If CO_2 electroreduction is limited by an irreversible concerted proton electron transfer step with HCO_3^- as the proton donor, the reaction rate expressed as a partial current for CO is:

$$j_{CO} = nFk\theta P_{CO_2} C_{HCO_3^-} \exp\left(\frac{\beta F\eta}{RT}\right)$$

This rate law shows a first-order dependence on both CO_2 and HCO_3^-. The Tafel slope is given by the partial derivative of the overpotential with respect to the logarithm of current, yielding:

$$\left(\frac{\partial\eta}{\partial \log j_{CO}}\right)_{P_{CO_2}, C_{HCO_3^-}} = \frac{2.3RT}{\beta F} = 118 \ \ \mathrm{mV/dec}$$

This proposed mechanism theoretically involves a Tafel slope of 118 mV/decade and a first order dependence on CO_2 and bicarbonate [1]; experimentally, we observe a 120 mV/decade Tafel slope, a 0.60 order dependence on CO_2, and a 1.40 order on bicarbonate (Table S5).

References

(1) Wuttig, A.; Yoon, Y.; Ryu, J.; Surendranath, Y. Bicarbonate Is Not a General Acid in Au-Catalyzed CO_2 Electroreduction. *J. Am. Chem. Soc.* **2017**, *139*, 17109–17113.

(2) Lobaccaro, P.; Singh, M. R.; Clark, E. L.; Kwon, Y.; Bell, A. T.; Ager, J. W. Effects of Temperature and Gas–Liquid Mass Transfer on the Operation of Small Electrochemical Cells for the Quantitative Evaluation of CO_2 Reduction Electrocatalysts. *Phys. Chem. Chem. Phys.* **2016**, *18*, 26777–26785.

(3) Hu, X.-M.; Rønne, M. H.; Pedersen, S. U.; Skrydstrup, T.; Daasbjerg, K. Enhanced Catalytic Activity of Cobalt Porphyrin in CO_2 Electroreduction upon Immobilization on Carbon Materials. *Angew. Chemie Int. Ed.* **2017**, *56*, 6468–6472.

(4) Zhang, X.; Wu, Z.; Zhang, X.; Li, L.; Li, Y.; Xu, H.; Li, X.; Yu, X.; Zhang, Z.; Liang, Y.; et al. Highly Selective and Active CO_2 Reduction Electrocatalysts Based on Cobalt Phthalocyanine/Carbon Nanotube Hybrid Structures. *Nat. Commun.* **2017**, *8*, 14675.

(5) Kramer, W. W.; McCrory, C. C. L. Polymer Coordination Promotes Selective CO_2 Reduction by Cobalt Phthalocyanine. *Chem. Sci.* **2016**, *7*, 2506–2515.

(6) Morlanés, N.; Takanabe, K.; Rodionov, V. Simultaneous Reduction of CO_2 and Splitting of H_2O by a Single Immobilized Cobalt Phthalocyanine Electrocatalyst. *ACS Catal.* **2016**, *6*, 3092–3095.

(7) Maurin, A.; Robert, M. Noncovalent Immobilization of a Molecular Iron-Based Electrocatalyst on Carbon Electrodes for Selective, Efficient CO_2-to-CO Conversion in Water. *J. Am. Chem. Soc.* **2016**, *138*, 2492–2495.

(8) Aoi, S.; Mase, K.; Ohkubo, K.; Fukuzumi, S. Selective Electrochemical Reduction of CO_2 to CO with a Cobalt Chlorin Complex Adsorbed on Multi-Walled Carbon Nanotubes in Water. *Chem. Commun.* **2015**, *51*, 10226–10228.

(9) Kornienko, N.; Zhao, Y.; Kley, C. S.; Zhu, C.; Kim, D.; Lin, S.; Chang, C. J.; Yaghi, O. M.; Yang, P. Metal–Organic Frameworks for Electrocatalytic Reduction of Carbon Dioxide. *J. Am. Chem. Soc.* **2015**, *137*, 14129–14135.

(10) Lin, S.; Diercks, C. S.; Zhang, Y.-B.; Kornienko, N.; Nichols, E. M.; Zhao, Y.; Paris, A. R.; Kim, D.; Yang, P.; Yaghi, O. M.; et al. Covalent Organic Frameworks Comprising Cobalt Porphyrins for Catalytic CO_2 Reduction in Water. *Science.* **2015**, *349*, 1208–1213.